PHYSICAL REVIEW E **67**, 016211 (2003)

Uniform semiclassical wave function for coherent two-dimensional electron flow

Jiří Vaníček[1] and Eric J. Heller[1,2]
[1]*Department of Physics, Harvard University, Cambridge, Massachusetts 02138*
[2]*Department of Chemistry and Chemical Biology, Harvard University, Cambridge, Massachusetts 02138*
(Received 30 August 2002; published 24 January 2003)

We find a uniform semiclassical (SC) wave function describing coherent branched flow through a two-dimensional electron gas (2DEG), a phenomenon recently discovered by direct imaging of the current using scanned probed microscopy [M.A. Topinka, B.J. LeRoy, S.E.J. Shaw, E.J. Heller, R.M. Westervelt, K.D. Maranowski, and A.C. Gossard, Science **289**, 2323 (2000)]. The formation of branches has been explained by classical arguments [M.A. Topinka, B.J. LeRoy, R.M. Westervelt, S.E.J. Shaw, R. Fleischmann, E.J. Heller, K.D. Maranowski, and A.C. Gossard, Nature (London) **410**, 183 (2001)], but the SC simulations necessary to account for the coherence are made difficult by the proliferation of catastrophes in the phase space. In this paper, expansion in terms of ''replacement manifolds'' is used to find a uniform SC wave function for a cusp singularity. The method is then generalized and applied to calculate uniform wave functions for a quantum-map model of coherent flow through a 2DEG. Finally, the quantum-map approximation is dropped and the method is shown to work for a continuous-time model as well.

DOI: 10.1103/PhysRevE.67.016211 PACS number(s): 05.45.Mt, 03.65.Sq, 73.23.−b

I. INTRODUCTION

There is no doubt that detailed understanding of the electron transport through mesoscopic devices is needed to take the full advantage of the possibilities of novel electronics these systems offer. On the experimental side, great progress was made with the use of scanned probe microscopes [1,3,4]. The theory has kept up: the present knowledge has already been summarized in several monographs [5–7].

Quantum effects have become central as devices have become smaller, cooler, and containing fewer impurities. Remarkably many quantum properties of the electron flow through nanostructures can be explained by semiclassical (SC) methods. These methods are based on classical mechanics: the relevant classical manifolds form the ''skeleton'' to which the wave function is attached [8]. The SC methods need to be substituted for classical ones when coherence is maintained over distances on the order of the size of the device, and when interference effects are playing a role.

In their simplest form, the SC techniques fail when nonlinear classical dynamics create complicated structures in phase space. In particular, the SC approximation breaks down whenever there are multiple contributions to the wave function within the volume of a single Planck cell. These so-called catastrophes have been classified [9,10] and various methods have been devised to correct the SC wave functions in cases when there exist only several coalescing contributions [11–13]. In the setting of mesoscopic devices, improved SC methods have been applied e.g., to the scattering through ballistic microstructures [14] or to the magnetotransport through a resonant tunneling diode [15].

In a recent paper [16], we successfully explored a new approach which worked even in situations with an infinite number of coalescing contributions, occurring e.g., in the case of the homoclinic tangle near an unstable periodic orbit [17]. This method is based on the idea of replacing a complicated classical manifold by a series of new simpler manifolds. When standard semiclassical methods are applied to these ''replacement manifolds'' (RMs), accurate uniform wave functions are obtained in situations where direct semiclassical evaluation of the original manifold fails miserably.

Originally, this method was used in special, although common cases with an infinite number of oscillations with the same phase-space area. Here we demonstrate that this special property is not necessary, and that a similar approach may be used more generally, even in cases with localized perturbations. In Sec. II, we briefly review the RM method from Ref. [16] and generalize it. The method is used to uniformize a cusp singularity in Sec. III. In Sec. IV, we apply the generalized method to find a uniform wave function in a quantum-map model of a 2D electron flow through a sample with impurities, where multiple cusp catastrophes are present. The quantum-map approximation is relaxed in Sec. V and it is shown how the replacement manifolds are formed in a continuous-time model. In Sec. VI, we discuss the merits of the RM method and relate it to other SC techniques. Because most of this paper is concerned with what happens to the twisted manifold under the shear of phase space, for completeness the Appendix addresses the other major phase-space motion: rotation.

II. REPLACEMENT-MANIFOLD METHOD AND ITS GENERALIZATION

The original method, discussed in detail in Ref. [16], works for wave functions of the form

$$\psi(q) = A(q) e^{iS(q)/\hbar} \tag{1}$$

with

$$S(q) = S_0(q) + \hbar \epsilon \sin f(q), \tag{2}$$

that can be associated with classical manifolds in which the momentum depends on the position as

$$p(q)=\frac{\partial S}{\partial q}=\frac{\partial S_0}{\partial q}+\hbar\epsilon f'(q)\cos f(q). \tag{3}$$

Here S_0 and S are the unperturbed and full action, respectively, ϵ is a parameter controlling the strength of the perturbation, $A(q)$ gives the local weight of the manifold, and $f(q)$ is a smooth function defining the shape of the perturbation.

We can expand the wave function as

$$\psi_{RM}(q)=\sum_{n=-\infty}^{\infty}A_n(q)\exp\left[\frac{i}{\hbar}S_n(q)\right], \tag{4}$$

and interpret each term of the sum as a contribution from a classical ''replacement'' manifold $p_n(q)=\partial S_n/\partial q$ with a weight $A_n=A(q)J_n(\epsilon)$ and an action $S_n(q)=S_0(q)+n\hbar f(q)$. The advantage of the RM expansion is appreciated after moving to the momentum representation with caustics where semiclassical form $\Sigma A_j^{SC}(p)\exp[iS_j^{SC}(p)/\hbar]$ fails while the sum over RMs gives an accurate result.

A slightly different and more general approach than in Ref. [16] does not require an oscillatory behavior of the action. If

$$S(q)=S_0(q)+\epsilon\Delta S(q), \tag{5}$$

we may Taylor expand the wave function as

$$\psi(q)=A(q)\exp\left[\frac{i}{\hbar}S_0(q)\right]\sum_{n=0}^{\infty}\frac{1}{n!}\left[\frac{i}{\hbar}\epsilon\Delta S(q)\right]^n$$

$$=\sum_{n=0}^{\infty}A_n(q)\exp\left[\frac{i}{\hbar}S_n(q)\right] \tag{6}$$

corresponding to RMs with weights

$$A_n(q)=A(q)(i\epsilon)^n/n!$$

and actions

$$S_n(q)=S_0(q)-i\hbar n\ln[\Delta S(q)/\hbar].$$

Defining a new function $f(q)$ by $\Delta S(q)\equiv\hbar\exp[f(q)]$, the nth RM action becomes

$$S_n(q)=S_0(q)-i\hbar n f(q). \tag{7}$$

It will help the convergence of expansion (6) if $\lim_{q\to\pm\infty}f(q)=-\infty$. This, however, is a natural property of localized perturbations.

The simplest nontrivial example is obtained by choosing $f(q)=-q^2$. Besides allowing an analytic solution, this choice will yield exactly the manifold needed in our model of a 2D electron flow in Sec. IV. Expanding the function $p(q)$ around $q=0$,

$$p(q)=-2\epsilon\hbar qe^{-q^2}\approx 2\epsilon\hbar(q^3-q)+O(q^4), \tag{8}$$

we find that this case falls into the second simplest universality class (called cusp) of catastrophe theory [9,10,18] (see Fig. 1).

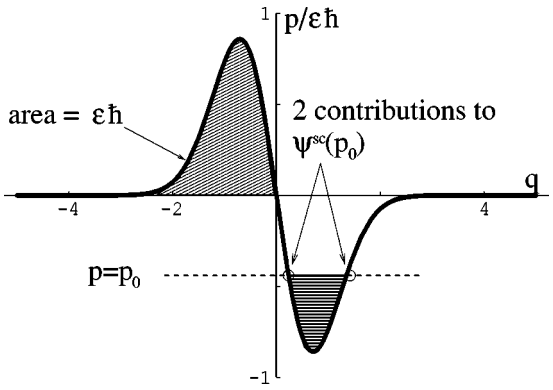

FIG. 1. Initial manifold of Eq. (8) and areas important to the semiclassical approximation of $\psi(p)$.

Assuming that the weighing of this manifold is $A(q)=\text{const}=(2\pi\hbar)^{-1/2}$, the corresponding SC wave function is

$$\psi_{SC}(q)=(2\pi\hbar)^{-1/2}\exp(i\epsilon e^{-q^2}). \tag{9}$$

Since for all positions q, there exists only a single contribution to $\psi_{SC}(q)$, the SC position wave function is accurate, $\psi(q)\approx\psi_{SC}(q)$, and the momentum wave function is given by the Fourier transform

$$\psi(p)=(2\pi\hbar)^{-1/2}\int dq\,\psi_{SC}(q)e^{-ipq/\hbar}. \tag{10}$$

Evaluating this integral by the stationary-phase (SP) approximation yields the SC momentum wave function $\psi_{SC}(p)$. The SC momentum wave function has two contributions from two SP points (Fig. 1). The horizontally filled-in area gives the phase between two contributions; if it becomes smaller than $\hbar$, the SP approximation breaks down. Therefore, $\psi_{SC}(p)$ will be singular for all classically allowed momenta when $\epsilon\leqslant 1$.

Note that the RM momentum $p_n(q)=2in\hbar q$ is purely imaginary for all q and that the corresponding manifold has no caustics. The uniform momentum wave function is found as

$$\psi_{RM}(p)=(2\pi\hbar)^{-1/2}\int dq\,e^{-ipq/\hbar}\sum_{n=0}^{\infty}A_n e^{iS_n(q)/\hbar}$$

$$=\delta(p)+\frac{\sqrt{\pi}}{2\pi\hbar}\sum_{n=1}^{\infty}\frac{(i\epsilon)^n}{n!}n^{-1/2}\exp\left(\frac{-p^2}{4n\hbar^2}\right) \tag{11}$$

$$=\delta(p)+\sum_{n=1}^{\infty}\tilde{A}_n e^{i\tilde{S}_n(p)/\hbar}, \tag{12}$$

where

$$\tilde{A}_n=\frac{\sqrt{\pi}}{2\pi\hbar}\frac{(i\epsilon)^n}{n!}n^{-1/2}, \tag{13}$$

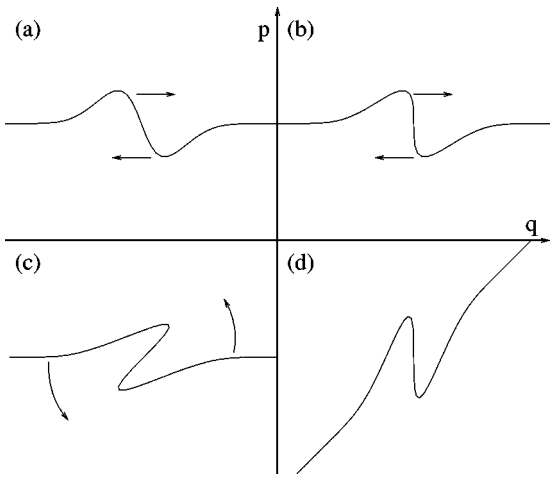

FIG. 2. An example of a manifold with the double loop structure that has been sheared (a-c) and rotated (c-d) in phase space. While shear and rotation are generic phase-space motions, here they were implemented by $H=p^2/2$ and $H=p^2/2+q^2/2$, respectively.

$$\tilde{S}_n(p)=-\int dp\, q_n(p)=\frac{ip^2}{4n\hbar}. \tag{14}$$

We can in general evaluate all RMs for $n\geqslant 1$ by the SP method, although in this case the answer turns out to be equal to the exact Fourier transform because the action S_n is quadratic.

III. UNIFORMIZATION OF A CUSP SINGULARITY

The formation of manifolds with a double-loop structure like that in Fig. 1 is a generic feature of nonlinear Hamiltonian systems. This pattern forms, for instance, whenever an ensemble of trajectories encounters a dip or a bump in the potential surface. Assuming that the particles have energy greater than the maximum of the potential, the dip or bump act as a convex or concave lens, respectively. After it is created, the double loop does not remain stationary: depending on the Hamiltonian, the structure will generally start to shear and rotate in phase space (see Fig. 2). In most of this paper we are concerned with the shear only, but for completeness, in the Appendix we present analytic formulas for the RM expansion of an original manifold that is arbitrarily rotated with respect to the q and p axes.

For now imagine that after the manifold (8) with two loops has been formed, the system evolves freely (with the Hamiltonian $H=p^2/2m$). The Hamilton's equations of motion are

$$\dot{q}=\frac{p}{m},$$

$$\dot{p}=0, \tag{15}$$

resulting in a shear of phase space. The SC position wave function, which was accurate at time $t=0$, will break down around time

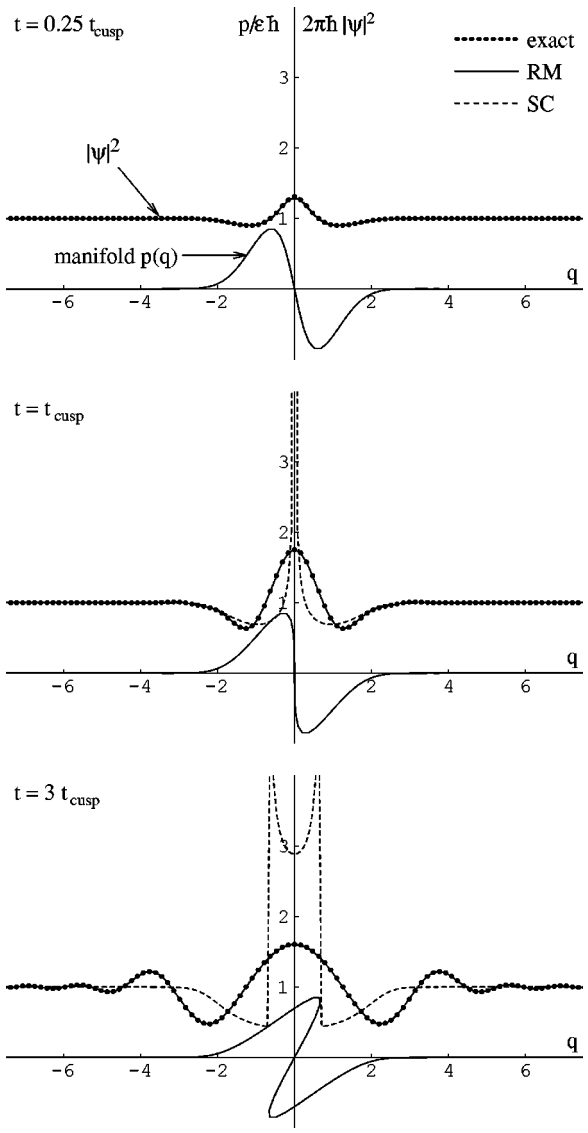

FIG. 3. Evolution of the manifold and the comparison of the exact (points), RM (solid line) and SC (dashed line) wave functions at a time instant before ($t=0.25\ t_{\rm cusp}$, top), at ($t=t_{\rm cusp}$, middle), and after ($t=3\ t_{\rm cusp}$, bottom) the cusp. In these plots, $\epsilon=1$ and the first five RMs were used in Eq. (20).

$$t_{\rm cusp}=\frac{m}{2\epsilon\hbar} \tag{16}$$

when a cusp singularity [13] develops (see Fig. 3).

This problem will be remedied if we apply any of the SC evolution methods (i.e., integration using the SP approximation) to the first few RMs instead of directly to the original manifold,

$$\psi_{RM}(q,t)=\int dq' K_f(q,q';t)\psi_{RM}(q',0)$$

$$=\sum_{n=0}^{\infty}\int dq' K_f(q,q';t)A_n e^{iS_n(q)/\hbar}, \tag{17}$$

where the free-space propagator

$$K_f(q'',q';t)=\left(\frac{m}{2\pi\hbar it}\right)^{1/2}\exp\left[\frac{im}{2\hbar t}(q''-q')^2\right] \quad (18)$$

and at $t=0$, using expression (6),

$$\psi_{RM}(q,0)=(2\pi\hbar)^{-1/2}\sum_{n=0}^{\infty}\frac{(i\epsilon)^n}{n!}e^{-nq^2}. \quad (19)$$

In our case, since the RM terms are Gaussian wave packets, their SC evolution (i.e., SP integration) can be performed analytically and is exact,

$$\psi_{RM}(q,t)=(2\pi\hbar)^{-1/2}\sum_{n=0}^{\infty}\frac{(i\epsilon)^n}{n!}(1+2in\hbar t/m)^{1/2}$$
$$\times\exp\left(\frac{-nq^2}{1+2in\hbar t/m}\right). \quad (20)$$

For comparison, the exact quantum evolution was performed by switching to the momentum representation, using the fast Fourier transform (FFT) and trivially evolving the wave function there. To find the primitive SC evolution, we used a method described by Berry *et al.* [19]. All the three methods are compared in Fig. 3, showing the classical manifold and corresponding exact, SC, and RM wave function at a time instant before, at, and after the cusp.

In the following section, we show that the RM method can treat situations in which more cusps are continuously formed. However, the advantage of the RMs over the Van Vleck propagation or other standard SC methods can be appreciated already when the rough region of the potential is localized in time and only one or a few cusps are created. As can be seen from Fig. 3, even if the potential is simply flat after certain time, the region of q in which the SC approximation breaks down expands. Unlike the simple SC approximation which deteriorates with time, the accuracy of the RM method is preserved after leaving the rough area of the potential: once the Gaussian wave packets corresponding to the RMs are formed, their number remains constant and their propagation is exact in any potential with up to quadratic terms (see Fig. 3).

IV. QUANTUM-MAP MODEL OF A 2D ELECTRON FLOW THROUGH A SAMPLE WITH IMPURITIES

We are now prepared to address the problem of the 2D electron flow in a semiconductor nanostructure with impurities. The electron transport in such a system is neither strictly ballistic nor strictly diffusive. Instead, the experiment has revealed that reality lies somewhere in between and the phenomenon has been termed ''branched flow [2].'' Figures 4 and 5 show, respectively the exact electron density (obtained by the exact quantum evolution using the FFT) and the representative classical trajectories in the model described below. The name of the phenomenon comes from the shape of the regions with enhanced electron density in Fig. 4 or the corresponding clusters of classical electron trajectories in Fig. 5. It turns out, however, that these do *not* correspond to the valleys in the potential [2]. Although the branches can already be seen in the classical simulations, Fig. 5 also shows that scattering by impurities leads to abundant cusp singularities in phase space, and therefore we expect deviations in both classical and primitive SC approximations from the exact quantum dynamics.

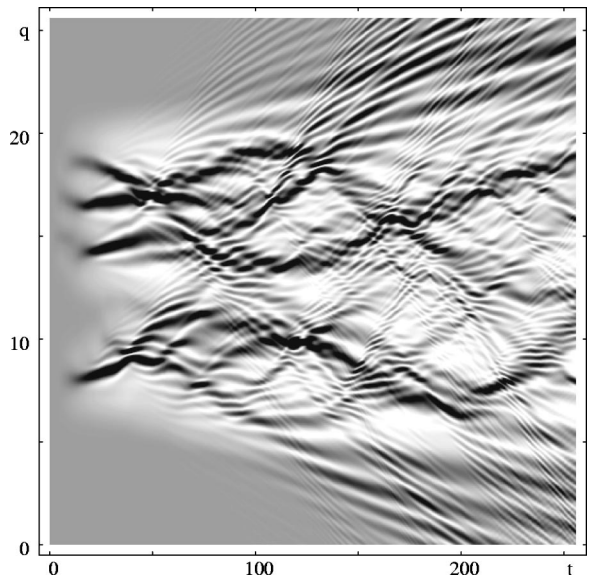

FIG. 4. Electron density $|\psi(q,t)|^2$ in the model of a 2D electron flow (obtained by the exact quantum evolution using the FFT, RMs were not used). For Hamiltonian, see Eq. (26). In this plot, $V_0/v=-0.0125$, $\epsilon=2.22$, and there were 256 impurities.

Here we analyze a simple model which can nevertheless exhibit all these properties. Namely, we discuss a 2D system with fast electrons, incident along the x axis and scattered by small isolated Gaussian impurities randomly distributed in the xy plane. Following Topinka and co-workers [1,2] who observed branched flow in a similar system, we consider the electron kinetic energy to be much larger than the amplitude

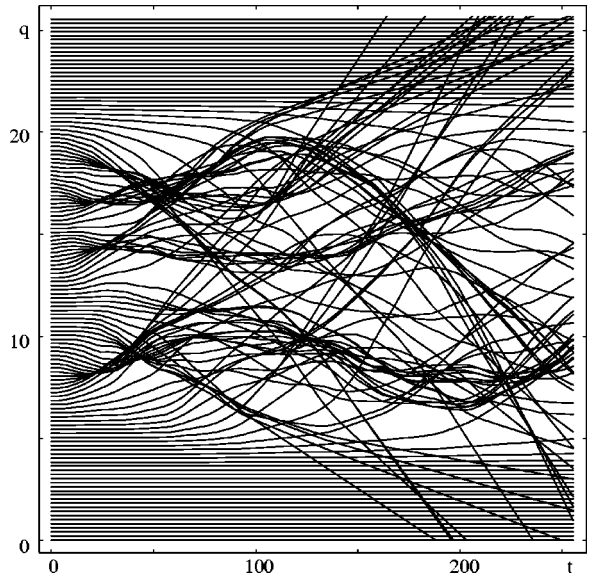

FIG. 5. Representative classical electron trajectories, corresponding to the electron density in Fig. 4.

of impurities. In fact, we assume the kinetic energy to be high enough to justify an impulse approximation: the electron propagates freely between effectively instantaneous kicks from impurities that affect its momentum but not position. Moreover, while the transverse momentum changes by a small impulse from an impurity, the longitudinal momentum remains effectively constant, allowing the transformation of the original 2D problem into a 1D problem with a time-dependent Hamiltonian. To be precise, we start with a 2D Hamiltonian

$$H(x,y,p_x,p_y)=\frac{p_x^2+p_y^2}{2m}+\sum_{j=1}^{n} V_0 \times\exp\left[-\frac{(x-x^{(j)})^2+(y-y^{(j)})^2}{a^2}\right], \tag{21}$$

where n, a, and $x^{(j)}$, $y^{(j)}$ are respectively the number, radius, and coordinates of the centers of the impurities. We assume that

$$\dot{x}=p_x/m\approx\text{const}=v, \tag{22}$$

where v is the initial velocity of the electron. This is justified when

$$mv^2/|V_0|\gg\sqrt{n}. \tag{23}$$

For simplicity of calculations, we distribute the impurities randomly in the y direction, but regularly along the x axis, at intervals $v\tau$. Each electron will be affected by a single impurity at a time if

$$v\tau\gg a. \tag{24}$$

To simplify notation, we take a, τ, and m to be respectively the units of length, time, and mass. Then we define dimensionless quantities $q=y/a$, $p=p_y\tau/ma$, etc. While we do not change the names of all other quantities, it should be understood that they have been made dimensionless as well. After this rescaling, we obtain an effective, 1D time-dependent Hamiltonian

$$H(q,p,t)=\frac{p^2}{2}+\sum_{j=1}^{n} V_0\ \exp[-(q-q^{(j)})^2-v^2(t-j)^2]. \tag{25}$$

In this section we consider that the change of the transverse momentum due to the impurity is instantaneous, yielding a further simplification, represented by a periodically ''kicked'' Hamiltonian

$$H(q,p,t)\approx\frac{p^2}{2}+\sqrt{\pi}\,\frac{V_0}{v}\sum_{j=1}^{n} e^{-(q-q^{(j)})^2}\delta(t-j). \tag{26}$$

(A generalized analysis without this approximation is presented in the following section.) In the impulse approximation, classical position q of an electron does not change during an interaction with jth impurity [20]. Classical dynamics may therefore be expressed in terms of a map,

$$q_{j+1}=q_j+p_j,$$
$$p_{j+1}=p_j+\Delta p(q_{j+1},q^{(j+1)}), \tag{27}$$

where subscripts denote time in units τ and the change of momentum is

$$\Delta p(q,q^{(j)})\approx-\int_{-\infty}^{\infty}dt\frac{\partial H}{\partial q}=2\sqrt{\pi}\,\frac{V_0}{v}(q-q^{(j)})e^{-(q-q^{(j)})^2}, \tag{28}$$

implying that a single impurity transforms a momentum state exactly into the two-loop manifold (8) from Sec. II. We can read off the loop area from Eq. (28) to be $\sqrt{\pi}|V_0|/v$.

In quantum mechanics, another important parameter enters: $\hbar$. Accuracy of the SC approximation will depend on how

$$\epsilon=\sqrt{\pi}\,\frac{|V_0|}{v\hbar} \tag{29}$$

compares to 1. In the impulse approximation, the exact quantum dynamics is described by a quantum map

$$|\psi_{j+1}\rangle=U|\psi_j\rangle, \tag{30}$$

where the subscript again denotes time in units τ and U is the one-step evolution operator

$$U=T\exp\left(-\frac{i}{\hbar}\int_0^1 H\,dt\right)\approx\exp\left(-\frac{i}{\hbar}\int_{-\infty}^{\infty}V\,dt\right)\times\exp\left(-\frac{i}{\hbar}\frac{p^2}{2}\right)=\exp(i\epsilon\,e^{-q^2})\exp\left(-\frac{i}{\hbar}\frac{p^2}{2}\right). \tag{31}$$

The easiest way to evolve a quantum state numerically is to use the FFT to switch back and forth between position and momentum representations and apply the impulsive part of U in q representation and the kinetic part of U in p representation.

We now demonstrate that not only do the replacement manifolds lack singularities (present in the classical and SC analysis), but that they can also correctly reproduce all the details of the exact quantum solution. When the next impurity is encountered, each wave packet develops a loop in its phase-space representation which would soon lead to a new cusp singularity. We therefore replace it with a series of simpler manifolds, as in Sec. III, avoiding this problem.

In our model we exploit the fact that the RM terms are Gaussian wave packets, allowing their analytic evaluation with only a slight generalization of the calculations in Sec. III. Each term in the RM sum at time j has a Gaussian form,

$$\psi_j(q)=c\,e^{aq-bq^2},\quad \text{Re}\ \ b>0. \tag{32}$$

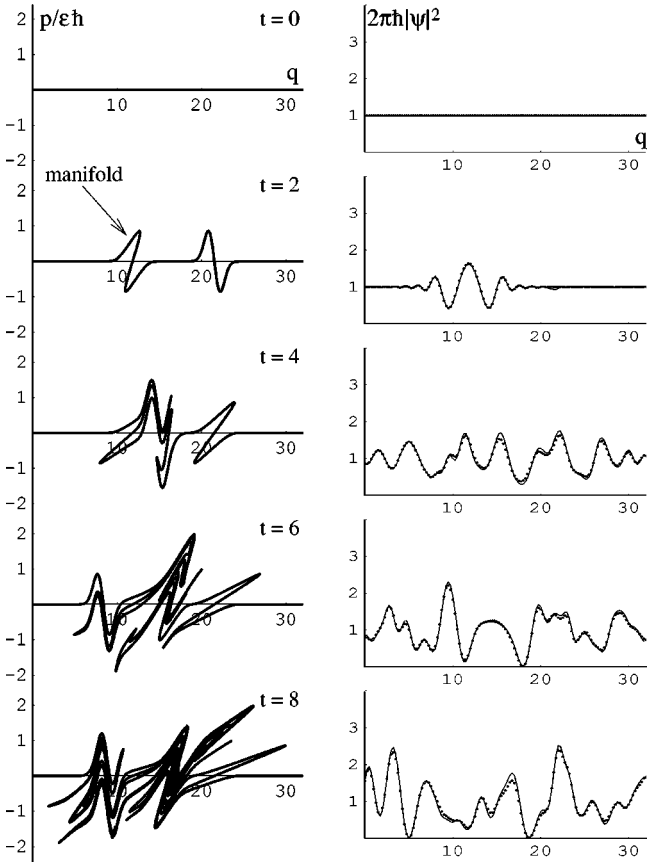

FIG. 6. Evolution of the manifold (left) and comparison of the corresponding exact (points) and RM (solid line) wave functions (right). The SC wave function is not shown since already at time $t=6$ it has caustic singularities almost everywhere along the q axis. In this plot, $V_0/v=-0.0625$ and $\epsilon=1.11$ was chosen to show that the RM method is not restricted to $\epsilon<1$. Only the first four RM terms were used in every step (34). Two new impurities were encountered at each time interval between the consecutive rows.

After the kinetic propagation, just before next impurity is encountered,

$$\tilde{\psi}_{j+1}(q)=\int K_f(q,q';1)\psi_j(q')dq' = \frac{c}{(1+2ib)^{1/2}}\exp\left(\frac{ia^2/2+aq-bq^2}{1+2ib}\right). \quad (33)$$

After receiving an impulse from the $(j+1)$st impurity,

$$\psi_{j+1}(q)=\tilde{\psi}_{j+1}(q)\exp[i\epsilon\, e^{-(q-q^{(j+1)})^2}] = \tilde{\psi}_{j+1}(q)\sum_{n=0}^{\infty}\frac{(i\epsilon)^n}{n!}\exp[-n(q-q^{(j+1)})^2]. \quad (34)$$

Each term in this sum gives rise to a new Gaussian wave packet of the form (32), which is propagated further in the same manner.

Figure 6 shows a comparison of the exact and RM evolution for $\epsilon=1.11$ up to a time when eight impurities are encountered. Four RMs are used to replace each incident wave packet at each impurity. Although the classical manifold (also shown in the figure) has developed many structures smaller than $\hbar$, the agreement remains excellent.

V. CONTINUOUS VERSION OF THE MODEL

In certain situations, we may be interested in a detailed evolution of the electron wave function during the collision with the impurity, rather than just in the appearance of the wave function after the collision. Below, we present an analytical solution of this problem in case that the electrons move slowly enough that the collision cannot be considered instantaneous, but fast enough that the transverse displacement of the electrons does not change significantly during the collision. (For even slower electrons, the coupling between the longitudinal and transverse motion during the collision would prevent us from obtaining closed analytic expressions presented below. However, we could still find the replacement manifolds numerically.)

To simplify the notation, we consider only a single impurity located at position $q=0$ and time $t=0$, so that the effective 1D time-dependent Hamiltonian (25) becomes

$$H(q,p,t)=\frac{1}{2}p^2+V_0\,\exp(-q^2-v^2t^2). \quad (35)$$

Assuming that q changes little during the collision we find that the momentum change is

$$\Delta p=p(t)-p(-\infty)=\int_{-\infty}^{t}dt'\dot{p}(t')=-\int_{-\infty}^{t}dt'\frac{\partial H}{\partial q} =2qV_0e^{-q^2}\int_{-\infty}^{t}dt'\exp(-v^2t'^2) =\sqrt{\pi}V_0v^{-1}qe^{-q^2}[1+\mathrm{erf}(vt)]. \quad (36)$$

At time $t=-\infty$, we start with a momentum eigenstate with momentum $p=0$,

$$\psi(p,t=-\infty)=\delta(p), \quad \text{or} \quad \psi(q,t=-\infty)=(2\pi\hbar)^{-1/2} \quad (37)$$

represented by a horizontal line in phase space. As the electron wave passes through the impurity, a double loop develops in the manifold (curve) representing the wave function. The position representation of the SC wave function at time t is (see, e.g., Ref. [19])

$$\psi(q_f,t)=(2\pi\hbar)^{-1/2}\left|\frac{dq_i}{dq_f}\right|^{1/2}\exp\left[\frac{i}{\hbar}(S_1+S_2)\right],$$

where q_i is the position at time $t'=-\infty$ that evolves to position q_f at time $t'=t$. In our approximation $q_f\approx q_i$, the Van Vleck determinant $|dq_i/dq_f|=1$, which is the reason that the SC position wave function remains accurate throughout

the collision. S_1 is the action along the trajectory of a reference point $q=x$ on the manifold,

$$S_1=\int_{-\infty}^{t} dt' L[x(t'),\dot{x}(t'),t'].$$

S_2 is the reduced action along the evolved manifold at time t,

$$S_2=\int_{x_f}^{q_t} dq_t' p_t(q_t')$$

[$p_t(q)$ is the momentum dependence on position at time t]. For convenience, we choose $x(-\infty)=-\infty$, giving $\dot{x}(t)=0$ and $x(t)=\text{const}=-\infty$. Since $V(x=-\infty,t)=0$, also $L(x,\dot{x},t)=0$ and $S_1=0$. Finally, since $p_{t=-\infty}(q)=0$,

$$S_2=\int_{-\infty}^{q} dq' \Delta p_t(q')=\sqrt{\pi}V_0 v^{-1}[1+\text{erf}(vt)] \times\int_{-\infty}^{q} dq' q' e^{-q'^2}=\sqrt{\pi}V_0 v^{-1}\frac{1}{2}[1+\text{erf}(vt)]e^{-q^2}. \tag{38}$$

The semiclassical position wave function at time t is

$$\psi_{SC}(q,t)=(2\pi\hbar)^{-1/2}\exp\left\{\frac{i}{\hbar}\sqrt{\pi}V_0 v^{-1}\frac{1}{2}[1+\text{erf}(vt)]e^{-q^2}\right\}. \tag{39}$$

Remembering that $\sqrt{\pi}V_0 v^{-1}\hbar^{-1}=\epsilon$ and that $\text{erf}(\pm\infty)=\pm\infty$, we can easily check that this general expression gives the correct limiting forms (37) and (9) at times $t=-\infty$ and $t=\infty$, respectively. The primitive SC momentum wave function [obtained by the SPA of the Fourier transform of Eq. (39)] fails for the same reasons as in Sec. II. If we expand $\psi_{SC}(q,t)$ in terms of RMs, and apply the SPA directly to the RMs, we find an accurate answer. The only difference from expression (11) is an extra factor $\{\frac{1}{2}[1+\text{erf}(vt)]\}^n$ for RM coefficients A_n or $\tilde{A}_n$ (13), e.g.,

$$\tilde{A}_n=\frac{\sqrt{\pi}}{2\pi\hbar}\frac{(i\epsilon)^n}{n!}n^{-1/2}\left\{\frac{1}{2}[1+\text{erf}(vt)]\right\}^n.$$

Since the expression in the large parentheses goes smoothly from 0 at $t=-\infty$ to 1 at $t=\infty$, we see that the replacement manifolds emerge even before the center of the impurity is encountered. However, the weight of the manifolds with larger n becomes appreciable only after the impurity is passed.

VI. DISCUSSION AND CONCLUSIONS

We have shown that the RM method is not limited to infinitely repeating phase-space structures if we allow the replacement manifolds to have complex momenta. Propagation of replacement manifolds gives uniform semiclassical wave functions long after the primitive semiclassical approximation breaks down.

Putting aside the accuracy, the RM approach may seem intimidating from a numerical point of view because as described, the algorithm has exponential complexity. But let us remember that the same—exponential proliferation of contributions—is true of the primitive semiclassical solution which, however, would give a completely wrong result in our case! Moreover, there appear to be at least two possible ways to speed up the RM calculations. For $\epsilon<1$, we could prune the contributions to keep only terms up to a certain ''total'' power of ϵ (which is different from keeping all terms up to a given power at each impurity). Or we could consolidate the number of wave packets after certain time by projecting on a suitable basis (because the exponentially growing number of RM terms is obviously over complete) and starting the RM propagation afresh.

The question of computational complexity would not even arise if we were interested in a system where the electron wave hits only one or a few impurities and after that propagates in a relatively smooth potential. The small number of Gaussian wave packets spawned at the last impurity would suffice for all subsequent times and the accuracy of the approximation would be preserved. As discussed in Sec. III, this should be contrasted with the standard SC approximation which deteriorates even when a manifold with a single cusp propagates in a flat potential (see Fig. 3).

Besides providing a uniform wave function the RM method gives an intuitive explanation of how quantum mechanics smooths out the classical detail. Moreover, in the present case of RMs with a complex momentum, the method appears to provide a link between the semiclassical perturbation approximations [21] and various Gaussian wave packet techniques [22–24], because replacement manifolds in the expansion (19) are nothing but Gaussian wave packets. One advantage of the RM method over other Gaussian wave-packet methods lies in that it gives an analytic expression for the coefficients of the wave packets. Other Gaussian wave packet methods (such as the frozen Gaussians [22], the Herman-Kluk propagator [23], and the full multiple spawning [24]) rely on variational or *ad hoc* methods to obtain optimal wave packet coefficients numerically.

Finally, although the RM method has not yet been fully generalized, the large variety of problems (in this paper and in Ref. [16]) it can solve suggests that the method (or at least, *the idea*) is more general.

ACKNOWLEDGMENTS

This research was supported by the National Science Foundation under Grant No. CHE-0073544 and by the Institute for Theoretical Atomic and Molecular Physics. One of us (J. V.) would like to acknowledge helpful discussions with D. Cohen and A. Mody.

APPENDIX: REPLACEMENT-MANIFOLD EXPANSION IN AN ARBITRARILY ROTATED COORDINATE SYSTEM

We show here that the RM expansion for the manifold studied in this paper can be found analytically in an arbi-

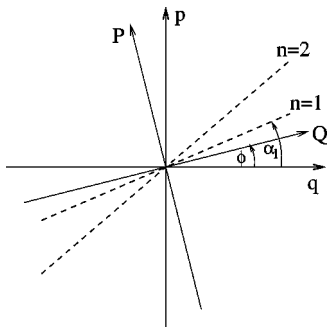

FIG. 7. Original and rotated coordinate systems.

trarily rotated coordinate system. In other words, the method can be readily applied not just in the q or p representations, but in any mixed representation given by a canonical transformation (see Fig. 7)

$$Q = q\cos\phi + p\sin\phi,$$

$$P = -q\sin\phi + p\cos\phi. \tag{A1}$$

In the original coordinate system $(q,\ p)$, replacement manifolds are straight lines

$$p_n(q) = 2in\hbar q = q\tan\alpha_n \tag{A2}$$

(where α_n is complex). In the rotated coordinates $(Q,\ P)$, the replacement manifolds are given by the relationship

$$P_n(Q) = Q\tan(\alpha_n - \phi) = Q\frac{2in\hbar - \tan\phi}{1 + 2in\hbar\tan\phi}. \tag{A3}$$

The reduced action is

$$S_n(Q) = \int dQ\, P_n(Q) = \frac{1}{2}Q^2\tan(\alpha_n - \phi). \tag{A4}$$

The weight of the nth RM in the Q representation is the weight in the q representation multiplied by the ratios of the projections on the q and Q axes, respectively. Including the Maslov index μ (0 or 1), we find the correct nth RM contribution

$$\psi_{RM,n}(Q) = \frac{1}{\sqrt{2\pi\hbar}}\frac{(i\epsilon)^n}{n!}\left|\frac{\cos\alpha_n}{\cos(\alpha_n - \phi)}\right|^{1/2} \times \exp\left[\frac{i}{2\hbar}Q^2\tan(\alpha_n - \phi) - i\mu_n\pi/2\right]. \tag{A5}$$

After simplification, the full RM expansion becomes

$$\psi_{RM}(Q) = \sum_{n=0}^{\infty}\psi_{RM,n}(Q) = \frac{1}{\sqrt{2\pi\hbar}}\sum_{n=0}^{\infty}\frac{(i\epsilon)^n}{n!}\left|\cos\phi + 2in\hbar\sin\phi\right|^{-1/2}\exp\left(-Q^2\frac{n + i\tan\phi/(2\hbar)}{1 + 2in\hbar\tan\phi} - i\mu_n\pi/2\right). \tag{A6}$$

It is easy to check that this general result correctly reduces to expressions (11) or (19) when $\phi = \pi/2$ or $\phi = 0$, respectively.

[1] M.A. Topinka, B.J. LeRoy, S.E.J. Shaw, E.J. Heller, R.M. Westervelt, K.D. Maranowski, and A.C. Gossard, Science **289**, 2323 (2000).

[2] M.A. Topinka, B.J. LeRoy, R.M. Westervelt, S.E.J. Shaw, R. Fleischmann, E.J. Heller, K.D. Maranowski, and A.C. Gossard, Nature (London) **410**, 183 (2001).

[3] M.A. Eriksson *et al.*, Appl. Phys. Lett. **69**, 671 (1996).

[4] R. Crook, C.G. Smith, C.H.W. Barnes, M.Y. Simmons, and D.A. Ritchie, J. Phys.: Condens. Matter **12**, L167 (2000).

[5] *Mesoscopic Electron Transport*, edited by L. L. Sohn, L. P. Kouwenhoven, and G. Schön (Kluwer Academic, Boston, MA, 1997).

[6] S. Datta, *Electronic Transport in Mesoscopic Systems* (Cambridge University Press, Cambridge, UK, 1997).

[7] Y. Imry, *Introduction to Mesoscopic Physics* (Oxford University Press, Oxford, UK, 1997).

[8] For standard semiclassical methods, see, e.g., M. Gutzwiller, *Chaos in Classical and Quantum Mechanics* (Springer, New York, 1990) or M. Brack and R. K. Bhaduri, *Semiclassical Physics* (Addison-Wesley, Reading, MA, 1997).

[9] R. Thom, *Structural Stability and Morphogenesis* (Benjamin, Reading, MA, 1975).

[10] V.I. Arnold, Usp. Mat. Nauk **30**, 3 (1975); Russ. Math. Surveys **30**, 1 (1975).

[11] G.F. Carrier J. Fluid Mech. **24**, 641 (1966).

[12] M.V. Berry, Proc. Phys. Soc. London **89**, 479 (1966).

[13] T. Pearcy, Philos. Mag. **37**, 311 (1946).

[14] L. Wirtz, J.-Z. Tang, and J. Burgdörfer, Phys. Rev. B **56**, 7589 (1997).

[15] E.E. Narimanov, A.D. Stone, and G.S. Boebinger, Phys. Rev. Lett. **80**, 4024 (1998).

[16] J. Vaníček and E.J. Heller, Phys. Rev. E **64**, 026215 (2001).

[17] For the definition of the homoclinic tangle, see, e.g., A. M. Ozorio De Almeida, *Hamiltonian Systems: Chaos and Quantization* (Cambridge University Press, Cambridge, UK, 1990).

[18] Another choice, $f(q) = -\frac{1}{4}q^4 + \frac{1}{2}q^2$, would give an example of another universality class: the so-called butterfly catastrophe.

[19] M.V. Berry, N.L. Balazs, M. Tabor, and A. Voros, Ann. Phys. (N.Y.) **122**, 26 (1979).

[20] With this approximation, the only classical parameter remaining is V_0/v.

[21] W.H. Miller and F.T. Smith, Phys. Rev. A **17**, 939 (1978).

[22] E.J. Heller, J. Chem. Phys. **75**, 2923 (1981).

[23] M.F. Herman and E. Kluk, Chem. Phys. **91**, 27 (1984).

[24] T.J. Martinez, M. Ben-Nun, and G. Ashkenazi, J. Chem. Phys. **104**, 2847 (1996); T.J. Martinez and R.D. Levine, Chem. Phys. Lett. **259**, 252 (1996).